Published in Mathematical Geosciences 44, issue 2, p.187-208, 2012
which should be used for any reference to this work

Multiphase Transport of Tritium in Unsaturated Porous Media—Bare and Vegetated Soils

J. Jiménez-Martínez · K. Tamoh · L. Candela · F.J. Elorza · D. Hunkeler

Abstract Tritium is a short-lived radioactive isotope ($T_{1/2} = 12.33$ yr) produced naturally in the atmosphere by cosmic radiation but also released into the atmosphere and hydrosphere by nuclear activities (nuclear power stations, radioactive waste disposal). Tritium of natural or anthropogenic origin may end up in soils through tritiated rain, and may eventually appear in groundwater. Tritium in groundwater can be re-emitted to the atmosphere through the vadose zone. The tritium concentration in soil varies sharply close to the ground surface and is very sensitive to many interrelated factors like rainfall amount, evapotranspiration rate, rooting depth and water table position, rendering the modeling a rather complex task. Among many exist-ing codes, SOLVEG is a one-dimensional numerical model to simulate multiphase transport through the unsaturated zone. Processes include tritium diffusion in both, gas and liquid phase, advection and dispersion for tritium in liquid phase, radioactive decay and equilibrium partitioning between liquid and gas phase. For its application with bare or vegetated (perennial vegetation or crops) soil surfaces and shallow or deep groundwater levels (contaminated or non-contaminated aquifer) the model has been adapted in order to include ground cover, root growth and root water uptake. The current work describes the approach and results of the modeling of a tracer test with tritiated water (7.3×10^8 Bq m^{-3}) in a cultivated soil with an underlying 14 m

J. Jiménez-Martínez · K. Tamoh · L. Candela
Department of Geotechnical Engineering and Geosciences, Technical University of Catalonia, 08034 Barcelona, Spain

J. Jiménez-Martínez (✉)
Geosciences Rennes UMR 6118 CNRS Université de Rennes 1, 35042 Rennes, France
e-mail: joaquin.jimenez-martinez@univ-rennes1.fr

F.J. Elorza
Department of Geological Engineering, Technical University of Madrid, 28003 Madrid, Spain

D. Hunkeler
Centre for Hydrogeology and Geothermic, University of Neuchâtel, 2000 Neuchâtel, Switzerland

deep unsaturated zone (non-contaminated). According to the simulation results, the soil's natural attenuation process is governed by evapotranspiration and tritium re-emission. The latter process is due to a tritium concentration gradient between soil air and an atmospheric boundary layer at the soil surface. Re-emission generally occurs during night time, since at day time it is coupled with the evaporation process. Evapotranspiration and re-emission removed considerable quantities of tritium and limited penetration of surface-applied tritiated water in the vadose zone to no more than ∼1–2 m. After a period of 15 months tritium background concentration in soil was attained.

Keywords Re-emission · Effective diffusion · Natural attenuation · Unsaturated zone · Tritium · Multiphase transport

1 Introduction

Tritium (^{3}H, half-life 12.33 yr), being chemically identical to hydrogen and thus interacting directly with water and organic substances, differs considerably in its behavior with respect to other radionuclides in the environment (Raskob 1995). Tritiated water can easily diffuse in free water and move unretarded with it, either in the liquid (HTO_l) or in the vapor phase (HTO_g) (Fig. 1). In a soil covered with vegetation, an important sink of the HTO_l stored in soil is the root water uptake, and subsequent loss of tritium by vapor exchange with the atmosphere through stomata (Kline and Stewart 1974). Consequently, plants play an important role in the detection and mapping of subsurface HTO_l (Richard and Kirby 1987; Kalisz et al. 1988; Richard and Price 1989) and HTO_g contamination (Andraski et al. 2005; Garcia et al. 2009).

Primary tritium migration integrates all the processes that jointly affect liquid water and vapor flow in the vadose zone (Phillips 1994). Thus, the tracer behavior represents a very robust indicator of water movement in soil. In arid regions, it has been suggested that solute diffusion in aqueous phase and in aqueous plus gas phase, when volatile (e.g. tritium), may be the principal mode of solute transport in the unsaturated zone (Barnes et al. 1994; Joshi et al. 1997; Scanlon 1992).

Modeling the alternate upward and downward transport of tritium in shallow unsaturated zone generally requires rather complex models and detailed input as concentration varies sharply and is very sensitive to many interrelated factors including rainfall amount, evapotranspiration rate, root depth or water table position. Besides, tritium presents a broad range of issues making modeling a complex task, among them vapor diffusion or thermally driven transport. Many numerical models, generally developed by atomic energy agencies to predict tritium migration throughout the unsaturated zone, exist. Such models, which have been compared by Barry et al. (1999) and Belot et al. (2005), are commonly used to predict the effect of tritiated rain or the re-emission of tritium from polluted groundwater to the atmosphere (Täschner et al. 1995). Some of them have been applied as well to calculate the absorbed mass by plants and food (organically bound tritium, OBT) (BIOMOVS II 1996). Common numerical models in hydrological studies, such as MACRO (Larsbo and Jarvis

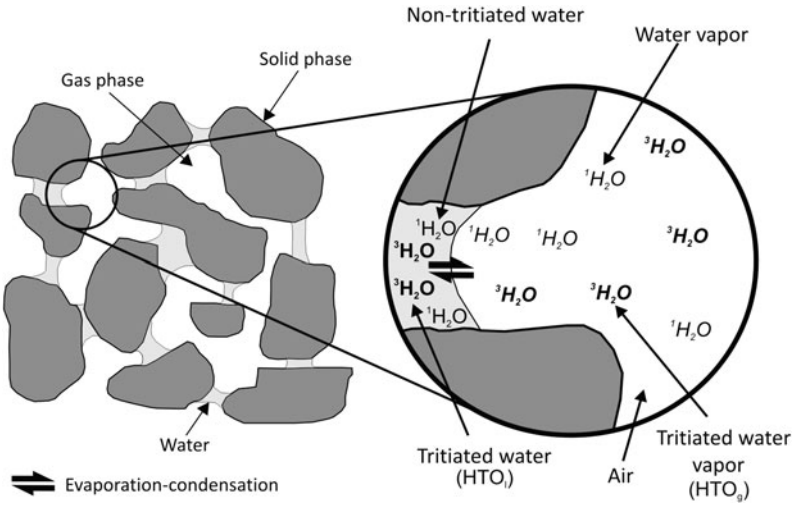

Fig. 1 Conceptual scheme for tritiated and non-tritiated water behavior in liquid and gas phase within an unsaturated porous media

2003) or TOUGH2 (Pruess et al. 1999), have also been used to simulate tritium transport through the vadose zone, but to a lesser extent. Many of these models work under monophasic and isothermal conditions or hardly consider the role played by plants.

The objective of this research was to quantify the upward and downward transport of tritium in a shallow unsaturated zone, as well as the natural soil attenuation process. A numerical modeling approach to simulate multiphase transport of tritium in unsaturated porous media is described. To evaluate the model performance, a field test with a tritiated water application on a vegetated soil surface has been carried out. For the modeling approach, SOLVEG (Yamazawa and Nagai 1997; Yamazawa 2001), a one-dimensional numerical model that simulates multiphase tritium transport through bare soil, was utilized after being modified for its use on vegetated soils.

2 Modeling Approach Description

The modeling approach is based on SOLVEG (Yamazawa and Nagai 1997; Yamazawa 2001), one-dimensional finite-difference model originally designed for bare soil, which solves the transport of heat, liquid water and vapor, tritiated liquid water (HTO_l) and vapor (HTO_g), and the soil-atmosphere exchange. In SOLVEG, advection and diffusion terms are resolved with an explicit and semi-implicit scheme, respectively. To adapt the code to the experimental conditions, it was modified in order to include ground cover, root growth and root water uptake processes. Radioactive decay was implemented also.

Although isotopically different, the HTO_l and H_2O molecules present similar behavior, therefore fractionation of hydrogen isotopes in water during root wa-

ter uptake can be assumed negligible, although exceptions exist for some plant species (Ellsworth and Williams 2007). On the contrary, differences exist between re-emission and evaporation processes. Re-emission is a mechanism that generally acts during night-time and is depending on the HTO_l content in the uppermost soil profile and the concentration of HTO_g in a boundary layer of atmospheric air adjacent to the soil surface. Tritium migration is thus driven by a concentration gradient across the soil/atmosphere interface. During day-time, the re-emission is coupled to the soil evaporation process (Täschner et al. 1997).

2.1 Water Transport: Liquid Flow and Vapor

The SOLVEG model simulates the water content θ ($\mathrm{L}^3\,\mathrm{L}^{-3}$) and the specific humidity of soil air W_a ($\mathrm{M}\,\mathrm{M}^{-1}$) along a soil profile. The equation for the water movement in the liquid phase is the classical Richards' type with additional sink/source terms including transpiration E_t ($\mathrm{M}\,\mathrm{L}^{-3}\,\mathrm{T}^{-1}$) (via root water uptake) and evaporation-condensation E_e ($\mathrm{M}\,\mathrm{L}^{-3}\,\mathrm{T}^{-1}$)

$$\frac{\partial\theta}{\partial t} = -\frac{1}{\rho_w}\left[\frac{\partial q}{\partial z} + (E_e + E_t)\right] \tag{1}$$

where q is the vertical liquid water flux ($\mathrm{M}\,\mathrm{L}^{-2}\,\mathrm{T}^{-1}$), ρ_w the water density ($\mathrm{M}\,\mathrm{L}^{-3}$), t the time (T), and z the vertical space coordinate (L).

The vertical flow of liquid water, q, is expressed as

$$q = -\rho_w\left[D(\theta)\frac{\partial\theta}{\partial z} + K(\theta)\right] \tag{2}$$

Unsaturated hydraulic conductivity $K(\theta)$ and water retention $h(\theta)$ functions were estimated using the power-law equations from Campbell (1974)

$$K(\theta) = K_s\left(\frac{\theta}{\theta_s}\right)^{2b+3} \tag{3}$$

$$h(\theta) = h_s\left(\frac{\theta}{\theta_s}\right)^{-b} \tag{4}$$

where b is the so-called pore size distribution index (–) and $2b + 3$ the pore disconnectedness index (–). The parameters h_s, θ_s and K_s are air entry potential (L), saturated water content ($\mathrm{L}^3\,\mathrm{L}^{-3}$), and saturated hydraulic conductivity ($\mathrm{L}\,\mathrm{T}^{-1}$), respectively. The soil water diffusivity $D(\theta)$ is expressed by

$$D(\theta) = K(\theta)\frac{\partial h}{\partial\theta} \tag{5}$$

The potential effects of barometric pumping on the advective transport of non-tritiated and tritiated water vapor were not considered (Auer et al. 1996). This simplification is justified because dispersion coefficients associated with barometric pressure fluctuations are 10^4 times smaller than molecular diffusion of non-tritiated and tritiated water vapor in air; therefore, diffusive transport should be more important than advective vapor transport at the shallow depths considered (Parker 2003). On the other hand, the relatively low temperatures considered in this study (i.e. less

than 80°C) enable to express the total water vapor flux as diffuse flux only (Bear and Gilman 1995). According to the previous paragraph, the equation for water vapor movement contains two terms, i.e. the diffusion and evaporation-condensation term

$$\frac{\partial[(\theta_s-\theta)W_a]}{\partial t}=\frac{\partial}{\partial z}\left[D_{wa}\tau_a(\theta)\frac{\partial W_a}{\partial z}\right]+\frac{E_e}{\rho_a} \tag{6}$$

where D_{wa} is the water vapor diffusion coefficient in air ($\mathrm{L^2\,T^{-1}}$), ρ_a the density of soil air ($\mathrm{M\,L^{-3}}$) as function of temperature, and $\tau_a(\theta)$ the tortuosity for soil air at θ (–); analogous to Jackson et al. (1974), the model uses $\tau_a(\theta)=(\theta_s-\theta)/1.5$.

The evaporation-condensation of water in soil is expressed as

$$E_e=\frac{\rho_a}{r_e(\theta)}\big[W_{\mathrm{sat}}(T_s)-W_a\big]\quad\text{when } W_{\mathrm{sat}}(T_s)>W_a \tag{7}$$

This expression is based on the concept that the driving force for soil evaporation-condensation is the difference between the specific humidity of the evaporating site (surface of soil water, W_{sat}) and that of the pore air, W_a. Evaporation is regulated by the density of soil air, ρ_a, and the evaporation resistance r_e ($\mathrm{T^{-1}}$). The latter parameter has been experimentally determined as function of θ for different soil types (Kondo and Saigusa 1994; Kondo and Xu 1997). It is assumed that water condensation occurs in a very short time, allowing W_a to become lower than or equal to W_{sat} at a given soil temperature (T_s). Whether the equilibrium condition between liquid and vapor phase is fulfilled, it is assessed from the characteristic times of vapor diffusion and liquid advection using a relationship described by Milly (1982). The thermally driven transport in the vapor phase is implicitly included in the model, since the gradient of the state variable W_a can be expanded in terms of water content and temperature according to Philip and de Vries (1957).

The boundary condition at the soil surface (1) is determined by the continuity of liquid water flux at ground surface (subscript X_0)

$$q_0=\begin{array}{ll} q_{s0}=-\rho_w K_s & \theta_0\geq\theta_{s0}\\ -(P+I)+E_r & \theta_0<\theta_{s0}\end{array} \tag{8}$$

where E_r is the amount of runoff ($\mathrm{M\,L^{-2}\,T^{-1}}$), P the precipitation ($\mathrm{M\,L^{-2}\,T^{-1}}$), I the irrigation ($\mathrm{M\,L^{-2}\,T^{-1}}$), and q_{s0} the maximum infiltration flux when the soil is saturated ($\mathrm{M\,L^{-2}\,T^{-1}}$). When soil water content equals or exceeds θ_{s0}, the model assumes water storage at the ground surface for any additional water added to the soil, therefore $E_r=0$.

The lower boundary condition corresponds to free drainage or constant head for deep or shallow water table, respectively. Hourly values of the areally averaged applied water intensity $(P+I)$ are used as input data. The boundary condition for the specific humidity, W_a, (6), can be determined according to

$$-\rho_a D_{wa}\tau_a(\theta)\frac{\partial W_a}{\partial z}\bigg|_{z=0}+E_{e0}=E_0 \tag{9}$$

where

$$E_{e0}=\int_{-\delta z_0}^{0}E_e\,dz \tag{10}$$

and

$$E_0 = \rho_a c_E |u_r| (W_{a0} - W_r) f(t) \tag{11}$$

This boundary condition assumes that water vapor flux from the ground surface to the atmosphere is composed of the sum of diffused water vapor flux from the inside of the uppermost soil profile and direct evaporation from the surface (δ_{z0} thick) in contact with the atmosphere. The parameter c_E is the bulk transfer coefficient (–), a thermodynamic coefficient dependent on wind velocity u_r ($\mathrm{L\,T^{-1}}$) among other meteorological variables (Matsushima and Kondo 1995), which permits to estimate the evaporation efficiency from a bare soil. W_r is the specific humidity of atmospheric air at the reference height ($\mathrm{M\,M^{-1}}$).

To represent the ground cover in the model, a sigmoid curve $f(t)$ has been implemented. For perennial vegetation, a constant value between 1 and 0, representing the surface fraction exposed, is considered. In cultivated areas, natural crop growth typically follows an S-shaped pattern. When a crop is first planted, ground cover is non-existent, potential evaporation is maximal, and thus $f(t) = 1$. On the contrary, when the crop reaches the mid-season growth stage, ground cover is complete, evaporation is effectively zero, and thereafter $f(t) = 0$. All that remains is specifying the transition from $f(t) = 1$ at planting to $f(t) = 0$ at the beginning of the mid-season growth stage.

2.2 Tritium Transport: Liquid Flow (HTO_l) and Vapor (HTO_g)

The transport equations for tritiated liquid water (HTO_l) and vapor (HTO_g) phase are

$$\frac{\partial[\theta C_w]}{\partial t} = -\frac{1}{\rho_w}\frac{\partial[qC_w]}{\partial z} + \frac{\partial}{\partial z}\left[D_T \frac{\partial C_w}{\partial z}\right] - (e_e + e_t) \tag{12}$$

$$\frac{\partial[(\theta_s - \theta)C_a]}{\partial t} = \frac{\partial}{\partial z}\left[D_{Ta}\tau_a(\theta)\frac{\partial C_a}{\partial z}\right] + e_e \tag{13}$$

where C_w and C_a are HTO_l and HTO_g concentration ($\mathrm{M\,L^{-3}}$), respectively. e_t is the plant transpiration of HTO_l from the soil ($\mathrm{M\,L^{-3}\,T^{-1}}$), calculated as the product of root water uptake and C_w at each depth. The evaporation-condensation term inside the soil, e_e ($\mathrm{M\,L^{-3}\,T}$), provides the link between (12) and (13)

$$e_e = \frac{\rho_a}{r_e(\theta)}\left[\frac{W_{\mathrm{sat}}(T_s)C_w}{\rho_w} - \frac{C_a}{\rho_a}\right] \tag{14}$$

As mentioned above for non-tritiated liquid water and vapor, this term is controlled by the evaporation resistance (r_e), and the thermally driven transport of tritiated water vapor is implicitly included.

The gas phase (13), as for non-tritiated water vapor, only includes a diffusion term, being D_{Ta}, the molecular HTO_g diffusion coefficient in air ($\mathrm{L^2\,T^{-1}}$), multiplied by the tortuosity. In the case of the liquid phase (12), it includes the advection and hydrodynamic dispersion D_T ($\mathrm{L^2\,T^{-1}}$), this last one is defined as the sum of effective diffusion D_p ($\mathrm{L^2\,T^{-1}}$) and mechanical dispersion D_d ($\mathrm{L^2\,T^{-1}}$)

$$D_T = D_p + D_d = \tau_w(\theta) D_{Tw} + \frac{\lambda q}{\rho_w} \tag{15}$$

D_p is a function of the molecular diffusion coefficient of tritiated liquid water in free solution, D_{Tw} ($\mathrm{L}^2\,\mathrm{T}^{-1}$), and the tortuosity of the medium as a function of water content τ_w, $D_p = \tau_w(\theta) D_{Tw}$. On the other hand, D_d is equal to the product of the seepage velocity v_s ($\mathrm{L}\,\mathrm{T}^{-1}$), $v_s = q/\theta$, and dispersivity λ (L), $D_d = \theta v_s \lambda$.

The upper boundary condition for tritiated liquid water, (12), is specified by an additional term only for the top layer (ground surface) expressing a gain of tritium due to water input. Mass dilution due to water input is indirectly accounted by the increase of θ on the left-hand side of the (12). Evaporation of HTO_l from ground surface to the atmosphere is expressed in a similar manner as that of non-tritiated liquid water

$$-D_{Ta}\tau_a(\theta)\frac{\partial C_a}{\partial z}\bigg|_{z=0} + e_{e0} = e_0 \tag{16}$$

where

$$e_{e0} = \int_{-\delta z_0}^{0} e_e \, dz \tag{17}$$

and

$$e_0 = c_E |u_r| (C_{a0} - C_r) f(t) \tag{18}$$

C_r is HTO_g concentration in atmospheric air at reference height ($\mathrm{M}\,\mathrm{L}^{-3}$).

2.3 Soil Temperature Profile

The thermal conductivity of soil is obtained according to McCumber and Pielke (1981), where the relationship between soil water potential, h, and soil thermal conductivity is nearly independent of soil type. This relation comes from fitting Al Nakshabandi and Kohnke's (1965) data.

To obtain the soil temperature profile, T_s (°K), a classical heat transport equation is solved including conduction, latent heat exchange (sink/source of heat) for soil water evaporation–condensation, and advection (convection) heat transport due to liquid water movement. The heat conduction through plant root was assumed negligible. The upper boundary condition for soil temperature is defined by a ground surface heat budget equation, whereas for the lower boundary condition, constant temperature is assumed.

2.4 Root Water Uptake and Root Growth

For the vegetation sub-model, SOLVEG has been modified in order to include ground cover, root growth and root water uptake processes. For ground cover, a sigmoid curve $f(t)$ has been used (Sect. 2.1). Proposed root water uptake and root growth model are described below. This new vegetation sub-model, in agreement with the process models available in the agronomic literature (Overman and Scholtz 2002; Campbell and Norman 1998), allows one to reduce the number of input parameters and data with respect to other models that have appeared in the literature (Nagai 2002).

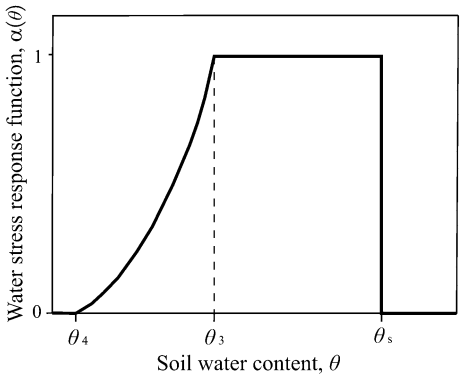

Fig. 2 Schematic of the plant water stress response function, $\alpha(\theta)$, modified from Feddes et al. (1978)

Root water uptake is considered a sink term of non-tritiated and tritiated water. A reference evapotranspiration ET_0 ($\mathrm{M\,L^{-2}\,T^{-1}}$) is obtained by the Penman–Monteith method (using hourly data). The potential evapotranspiration ET_p ($\mathrm{M\,L^{-2}\,T^{-1}}$) was calculated using a crop specific coefficient K_c (–), $ET_p = K_c \cdot ET_0$, which characterizes plant water uptake and evaporation relative to the reference vegetation (Allen et al. 1998). K_c can be considered constant for perennial vegetation, whereas in cultivated areas it changes in terms of growth stages. Once the potential transpiration, T_p ($\mathrm{M\,L^{-2}\,T^{-1}}$)—defined as water removed from soil due to plant water uptake—is obtained, for example using the approach of Kroes and Van Damm (2003), Pachepsky et al. (2004) or Jiménez-Martínez et al. (2009), it is then equally distributed over the soil root zone, z_{root} (L). This sink term was computed in the present paper by a method introduced by Campbell and Norman (1998) based on soil water content. Actual transpiration, E_t, is calculated according to

$$E_t(\theta) = \alpha(\theta)\frac{T_p}{z_{\mathrm{root}}} \tag{19}$$

where $\alpha(\theta)$ is the dimensionless water stress response function ($0 \leq \alpha \leq 1$) describing water uptake reduction due to drought stress. For $\alpha(\theta)$, a modified functional form introduced by Feddes et al. (1978) is applied (Fig. 2), where θ_3 and θ_4 are threshold parameters such that uptake is at the potential rate when the water content is between θ_3 and θ_s, it drops off when $\theta < \theta_3$, and becomes zero for $\theta < \theta_4$ or $\theta = \theta_s$.

While for perennial vegetation a constant root depth can be considered, a root growth model is required for crops. The model developed here assumes the classical Verhulst–Pearl logistic growth function (Šimunek et al. 2005), and the maximum depth is achieved at the end of the crop development stage.

3 Field Test for Model Validation

3.1 Experimental Setup

In order to evaluate the model performance, a field test was conducted in the Campo de Cartagena (SE Spain). The experiment took place from 17 June 2007 to 21 August 2008, along 429 days.

Table 1 Summary table of soil physical properties (mean ± standard deviation). ρ_s: soil bulk density; θ_s: saturated water content

Depth (cm)	Textural fractions (%)			ρ_s (kg m^{-3})	θ_s (m^3 m^{-3})
	Sand	Silt	Clay		
15	18.71 ± 2.26	75.95 ± 2.81	3.52 ± 1.57	1.45 ± 0.10	0.411 ± 0.029
45	13.80 ± 1.34	80.21 ± 2.05	5.98 ± 0.70	1.52 ± 0.11	0.378 ± 0.024
75	19.45 ± 2.79	77.16 ± 0.82	3.29 ± 2.11	1.58 ± 0.05	0.378 ± 0.015
150	10.82 ± 2.67	82.02 ± 1.20	6.57 ± 1.04	1.70 ± 0.08	0.320 ± 0.049

Table 2 Summary of soil hydraulic properties, flow and transport parameters. Threshold values for root water uptake reduction parameters (θ_3 is shown for two different crops)

Property		Value	Unit
Soil hydraulic properties			
Saturated water content	θ_s	0.372	m^3 m^{-3}
Air entry potential	h_s	-0.759[ab]	m
Saturated hydraulic conductivity	K_s	0.208×10^{-5}	m s^{-1}
Pore size distribution index	b	5.33[c]	–
Flow and transport (liquid and gas phase)			
Water density	ρ_w	1000	kg m^{-3}
Water vapor diffusion coeff. in air	D_{wa}	2.60×10^{-5}[d]	m^2 s^{-1}
Molecular HTO$_g$ diffusion coeff. in air	D_{Ta}	2.47×10^{-5}[e]	m^2 s^{-1}
Molecular HTO$_l$ diffusion coeff. in water	D_{Tw}	2.24×10^{-9}[f]	m^2 s^{-1}
Dispersivity of HTO$_l$	λ	0.01	m
Vegetation			
Threshold for root water uptake reduction	θ_3	0.259–0.270[g]	m^3 m^{-3}
Wilting point	θ_4	0.154[g]	m^3 m^{-3}

[a]Clapp and Hornberger (1978); [b]Cosby et al. (1984); [c]Campbell and Shiozawa (1992); [d]Cussler (1997); [e]Mayers et al. (2005); [f]Mills (1973); [g]Wesseling et al. (1991) and Taylor and Ashcroft (1972)

An experimental plot measuring 7 × 2 m was established on a cropped soil. Bulk density according to Grossman and Reinsch (2002), grain size distribution following Gee and Or (2002), and θ_s were analyzed at different depths up to 2 m depth (Table 1). Additional soil hydraulic properties and flow and transport parameters were taken from the literature (Table 2). The soil is a silty loam (USDA classification system), and the groundwater level was located at a depth of 14 m below the surface. The plot was managed according to common agricultural practices of the region, including crop rotation (lettuce and melon, Table 3), drip irrigation, and the application of a plastic cover during summer cropping to reduce direct evaporation from the ground surface. In order to avoid boundary effects, the plot sides were also cultivated with the same crops and equal agricultural management conditions were applied.

Table 3 Chronogram for the different crops and fallow periods. P: precipitation; I: irrigation

Description	Plant date	Harvest date	Length (days)	P (mm)	I (mm)
Melon crop	May 17, 2007	September 10, 2007	116	32	557
Fallow period	–	–	15	10	–
Lettuce crop	September 25, 2007	December 24, 2007	90	187	206
Fallow period	–	–	10	19	–
Lettuce crop	January 3, 2008	April 2, 2008	90	42	123
Melon crop	April 3, 2008	August 21, 2008	140	80	617

3.2 Tritium Input and Monitoring System

On 17 June 2007 (DAI 0, understanding DAI as day after injection), 12 L of tritiated water solution, with a concentration 7.3×10^8 Bq m^{-3}, was sprinkled (simulating rainfall) over the plot. The tritiated solution was prepared in the field site previously to the application. The soil profile monitoring for tritium transport was carried out by destructive sampling to obtain soil cores through a hand drilling auger; sampling depth increased as function of the time. Soil samples from cores were taken at regular depth intervals (being representative for a depth interval of 10 cm) (Fig. 3). In order to prevent the contamination from overlying layers, soil samples were taken from the inner part of the core, and immediately stored in leak proof bottles and transported in iceboxes to avoid tritium loss by evaporation. The data collection was divided into two periods: the first one, from 17 June to 10 September 2007 (DAI 0-83), shorter and intensive, for model calibration; the purpose of the second one was to evaluate the model performance, and included data from 11 September 2007 to 21 August 2008 (DAI 84-429). Hourly meteorological data were available from a weather station (SIAM 2008) located 235 m from the experimental plot. Measurements of background tritium concentration in precipitation were obtained from a station located 15 km NE from the field site, which is included in the Global Network Isotopes in Precipitation (GNIP/IAEA 2009).

To obtain enough centrifuged volume for tritium analysis, de-ionized water was added to the soil samples, which were subsequently tumbled to equilibrate the added water with the original pore water (Roy et al. 1991). Supernatant water was distillated to eliminate coloration, organic matter, and salts that could interfere with the analysis. The distilled samples were then mixed with a scintillation solution (Ultima Gold LLT) (Thatcher et al. 1977). Finally, the samples were analyzed at the CEDEX-Isotopic Techniques Laboratory (Spanish Government) using a liquid scintillation alpha-beta spectrometer (Tri-Carb 2560 TR/XL, Packard Instruments), which enables the measurement of low-level radioactivity (90 ± 40 Bq m^{-3}).

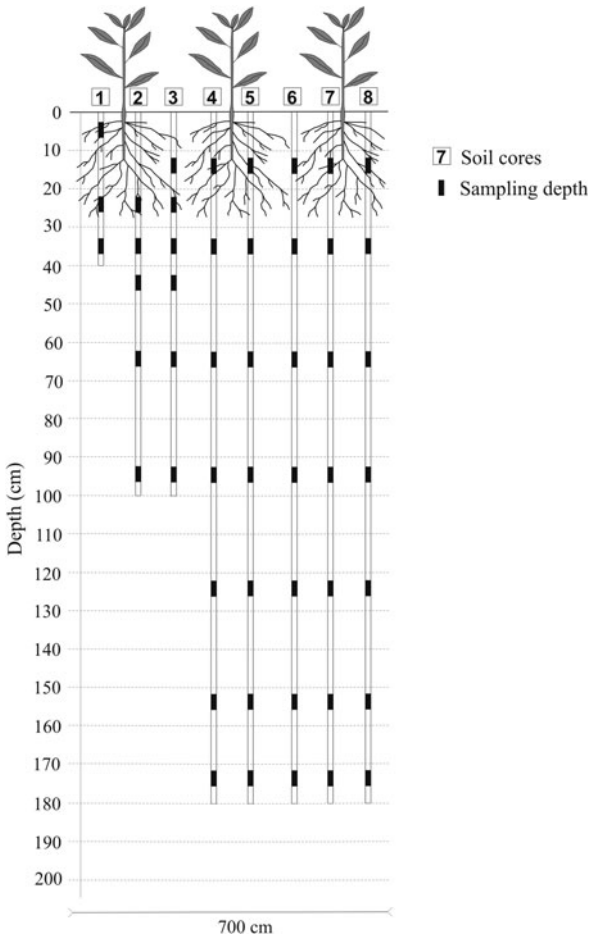

Fig. 3 Soil sampling locations along the soil profile

4 Results and Discussion

4.1 Model Calibration and Prediction

For the first sampling period (DAI 0-83), corresponding to the most intensive data collection and used for model calibration, a poor agreement of field data and simulations was attained with the initial input parameters (Table 2). Then, a manual calibration process was carried out, where several parameterizations were considered by varying the number and types of parameter to fit ($\theta_s, h_s, K_s, b, \lambda$), whereas the rest of the parameters included in Table 2 and obtained from literature (ρ_w; D_{wa}; D_{Ta}; D_{Tw}; θ_3; θ_4) were assumed fixed. Based on the mean relative error (*MRE*) as objective function, the best parameterization was achieved following the parsimony principle (as few fitted parameters as possible, Burhmam and Anderson 2002). The most influential parameters were found to be saturated hydraulic conductivity K_s, and dispersivity λ (Table 4).

Table 4 Fitted parameters values

Parameter	Initial value	Fitted value
Saturated hydraulic conductivity, K_s (m s^{-1})	0.208×10^{-5}	0.868×10^{-5}
Dispersivity coefficient, λ (m)	0.01	0.10

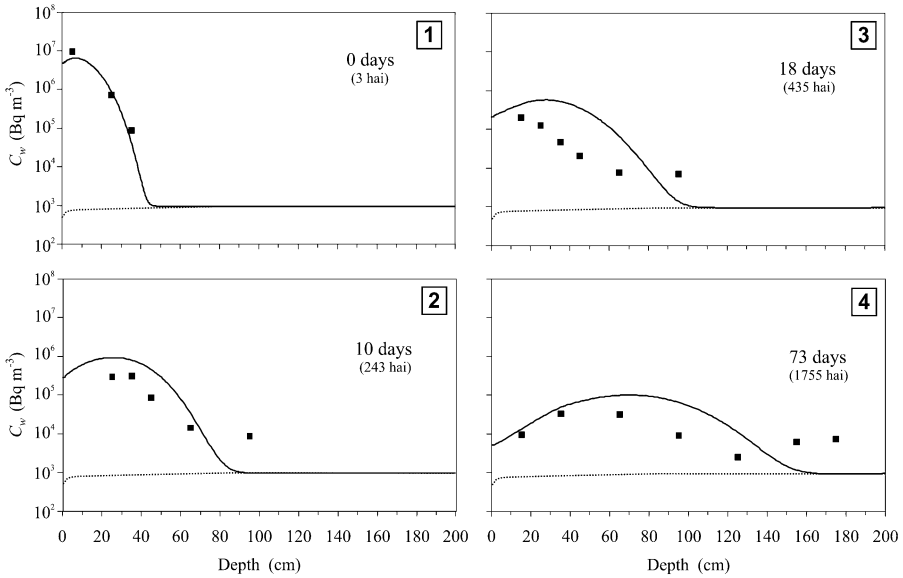

Fig. 4 Comparison between field data (*points*) and simulations (*solid lines*) for calibrated period (DAI 0-83). HTO_l background concentration (*dotted line*). Soil core according to Fig. 3 is indicated in box. hai: hours after injection

In Fig. 4 measured and simulated HTO_l concentration (C_w) profiles, for the calibrated period (DAI 0-83) are shown. A strong decrease of three orders of magnitude in HTO_l soil concentration can be recognized for this period. A good fit is obtained between simulated HTO_l concentration profiles and field data, despite the measurements being relatively sparse and the maximum concentration decreasing strongly. Subsequently, the second sampling period (DAI 84-429) was used to assess model performance (Fig. 5). The goodness-of-fit for calibrated and predicted period was evaluated through several statistics (Table 5).

The presence of HTO_l at greater depths than those obtained by simulation (Figs. 4 and 5) can be explained by preferential flow generation through roots and cracks within the first centimeters of the soil profile (tilled soil) at the beginning of the experiment (after tritiated water application).

4.2 Water and Tritium. Flux and Mass Balance

In Fig. 6, liquid water and vapor fluxes (tritiated and non-tritiated) after a water pulse of 8.4 mm (L m^{-2}) applied in 50 minutes, which took place 11 July 2007 at 12 a.m.

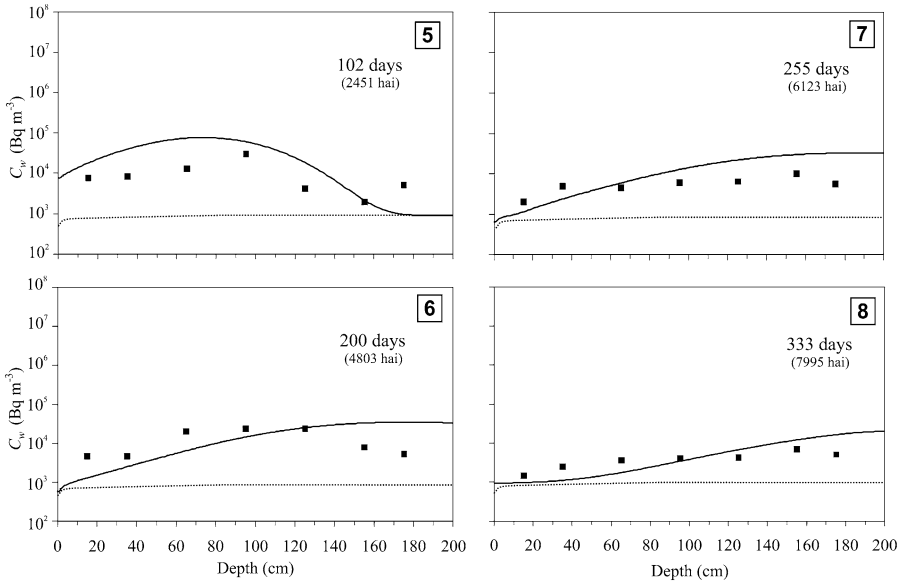

Fig. 5 Comparison between field data (*points*) and simulations (*solid lines*) for predicted period (DAI 84-429). HTO_l background concentration (*dotted line*). Soil core according to Fig. 3 is indicated in box. hai: hours after injection

Table 5 Goodness-of-fit for calibration and validation period (all field measurements were weighted equally)

Simulation	n		$RMSE$[a] (Bq m^{-3})	MAE[b] (Bq m^{-3})	MRE[c]
Calibration (DAI 0-83)	21	Input parameters	853497.9	329968.6	0.620
		Model fit	785158.1	326002.7	0.580
Validation (DAI 84-429)	28		17817.2	11370	0.681

[a]Root mean square error, $RMSE = \sqrt{\frac{1}{n}\sum_{i=1}^{n}(x_i - y_i)^2}$

[b]Mean absolute error, $MAE = \frac{1}{n}\sum_{i=1}^{n}|x_i - y_i|$

[c]Mean relative error, $MRE = \frac{\frac{1}{n}\sum_{i=1}^{n}|x_i - y_i|}{\frac{1}{n}\sum_{i=1}^{n}|y_i|}$

(DAI 22), have been plotted. In the numerical simulations of liquid water and vapor fluxes, for both tritiated and non-tritiated, the sign convention was negative fluxes-upward and positive fluxes-downward. The results show that the soil depth most affected by temperature, evaporation and root water uptake, corresponds to the upper 30 cm.

For the plotted period, Fig. 6(a) shows a large downward liquid water flux (q_w) in the top 30 cm during the first day (DAI 22), when the water pulse was applied, whereas for the rest of days q_w was upward by capillarity due to evaporation. The

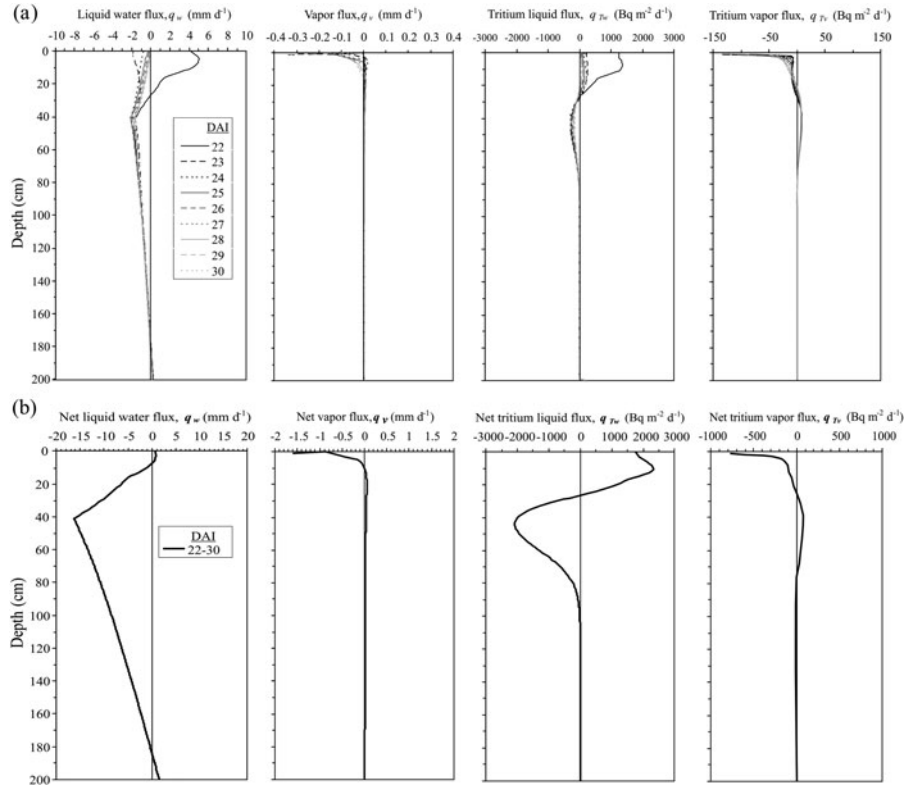

Fig. 6 (**a**) Computed liquid water (q_w) and vapor (q_v) flux expressed as water column (volumetric flux, 1 mm d^{-1} = 1 kg m^{-2} d^{-1}), and computed tritium liquid (q_{Tw}) and vapor (q_{Tv}) flux (mass flux, Bq m^{-2} d^{-1}) for a water pulse along 8 days (from 11 to 19 July 2007, DAI 22-30). (**b**) Net fluxes ($\boldsymbol{q}$) calculated for the mentioned period

depth reached by the roots until that moment is clearly recognized (40 cm). An upward vapor flux (q_v) up to a certain depth and a daily increasing trend is observed due to the drying process on the top soil. Below this evaporation front, until 110 cm depth, a downward q_v (Scanlon 1992; Gran et al. 2011) with lower magnitude than upward flux was produced. A similar trend was found for tritium liquid (q_{Tw}) and vapor (q_{Tv}) mass fluxes. A downward q_{Tw} up at 25–30 cm depth and upward between 30 and 90 cm depth are observed. On the contrary, q_{Tv} presents an opposite behavior, and it is remarkable the large upward q_{Tv} between 4 and 0 cm depth. Total or net fluxes ($\boldsymbol{q}$) for the mentioned period (DAI 22-30) are shown in Fig. 6(b). Net vapor flux ($\boldsymbol{q}_v$) was one order of magnitude lower than net liquid water flux ($\boldsymbol{q}_w$). A greater net tritium liquid flux ($\boldsymbol{q}_{Tw}$) than vapor ($\boldsymbol{q}_{Tv}$) can be recognized, although the interface between downward and upward mass flux, and the plane of zero mass flux, occurs at the same depth for both phases, at 27 and 100 cm depth, respectively.

Figure 7 illustrates daily tritium fluxes associated with evaporation and transpiration for the calibrated period (DAI 0-83). For the first eleven days following the tritiated water application, evaporation was the main process removing tritium from

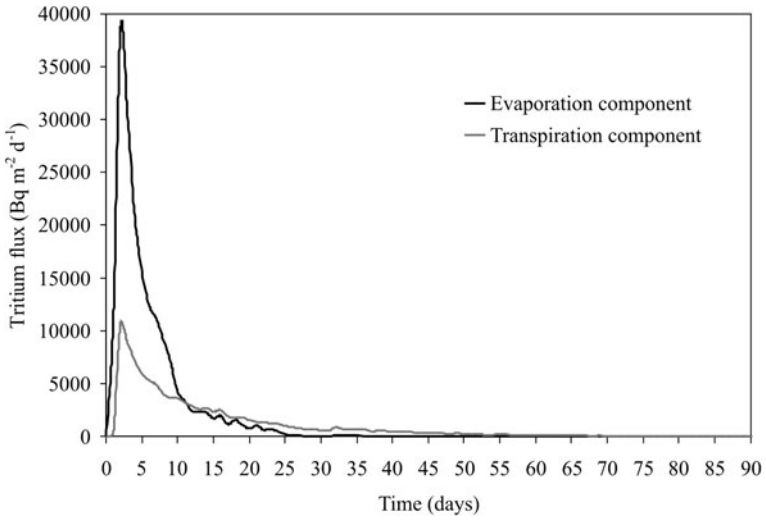

Fig. 7 Tritium flux, evaporation and transpiration component, to the atmosphere from 14 m^2 study area

the soil; after this moment, transpiration becomes the main sink of tritium. The tritiated water penetration and the increasing root depth, in the case of crops, determine the plants as the main sink and contributor to natural attenuation.

In order to establish an accurate soil water balance, water inputs (precipitation plus irrigation), losses by transpiration, evaporation and drainage, and changes in soil water storage were considered as main components. Figure 8(a) shows cumulative computed values for the mentioned water balance components. As the main objective of this work was to establish an accurate tritium mass balance, the cumulative tritium activity of each water balance component for liquid and vapor phase were considered: activity in liquid and vapor phase; evaporated and transpired tritium; and radioactive decay (Fig. 8(b)). The loss of tritium activity in soil after 83 days (1992 hours) was 95%, at the end of the field test, the background HTO_l concentration in soil ($\sim$950 Bq m^{-3}) was practically recovered. The tritium mass (activity) balance error, from simulations and for the total simulated period, was 0.5%.

4.3 Tritium Transport Processes

The HTO_l transport includes the advection and hydrodynamic dispersion (D_T) terms (1 1). D_T is defined as the sum of effective diffusion (D_p) and mechanical dispersion (D_d) (Sect. 2.2). While advection controls the transport of HTO_l in all soil profile, mechanical dispersion decreases with depth and effective diffusion is more or less constant along the profile (Fig. 9). According to Maraqa et al. (1997), the impact of effective diffusion on hydrodynamic dispersion, under unsaturated conditions, is not significant.

Transport of HTO_g only includes the diffusion term, also called effective diffusion (13). A diurnal variation in HTO_g concentration (C_a) directly related to meteoro-

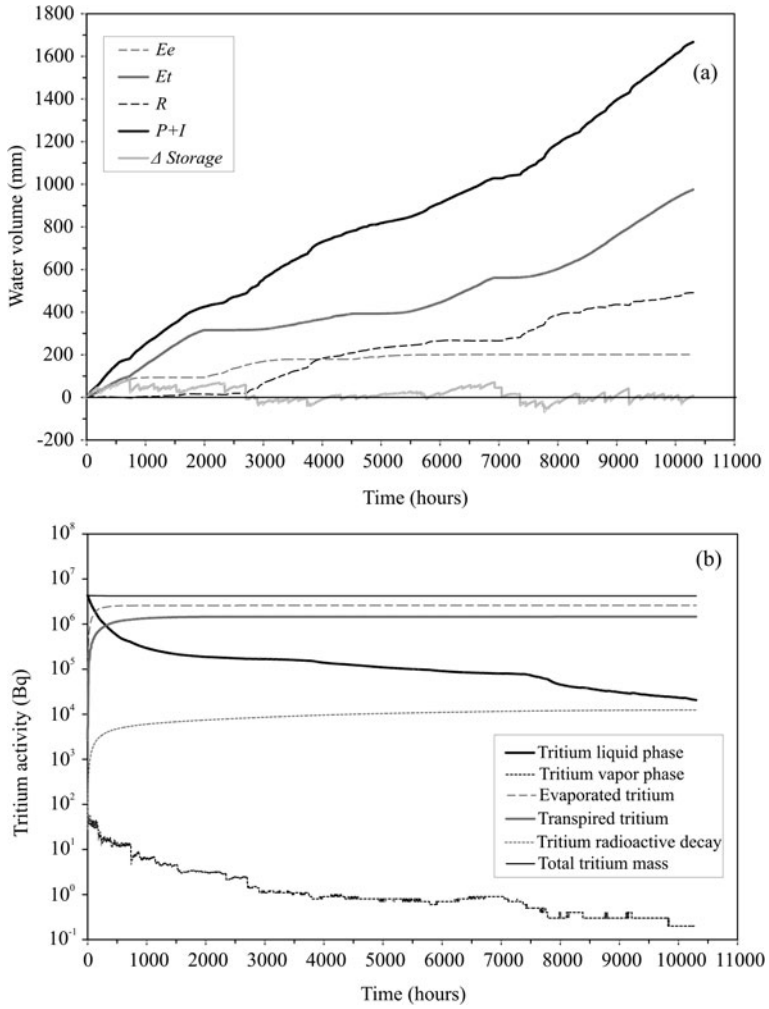

Fig. 8 (**a**) Cumulative volume expressed as water column (mm) for each water balance component (E_e: evaporation; E_t: transpiration; R: deep drainage; $P + I$: precipitation plus irrigation; $\Delta Storage$: soil water storage). (**b**) Tritium activity included in each water balance component and phase, it involves: tritium activity in liquid and gas phase, evaporated and transpired tritium, and radioactive decay

logical parameters, along with a trend to decrease with depth, is found (Fig. 10). Soil heat storage at day time favors HTO_l evaporation to HTO_g in the soil media. Subsequently, at sunset, condensation begins (14). In the top soil, the decline of HTO_g concentration during night time is reinforced by night re-emission, a phenomenon clearly observed during the previous simulation exercise at the injection date (Fig. 11). After a large volume application of water (precipitation or irrigation), the increasing HTO_g concentration at higher depth is due not only by the downward flux of HTO_l, but also by downward molecular HTO_g diffusion (13) (Fig. 10).

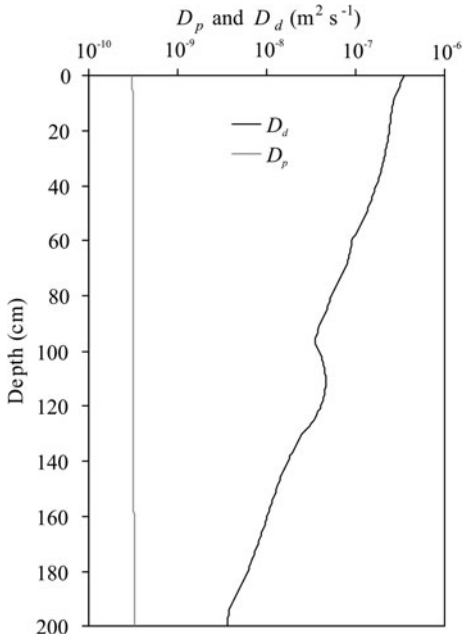

Fig. 9 Mean value along the soil profile for effective diffusion (D_p) and mechanical dispersion (D_d)

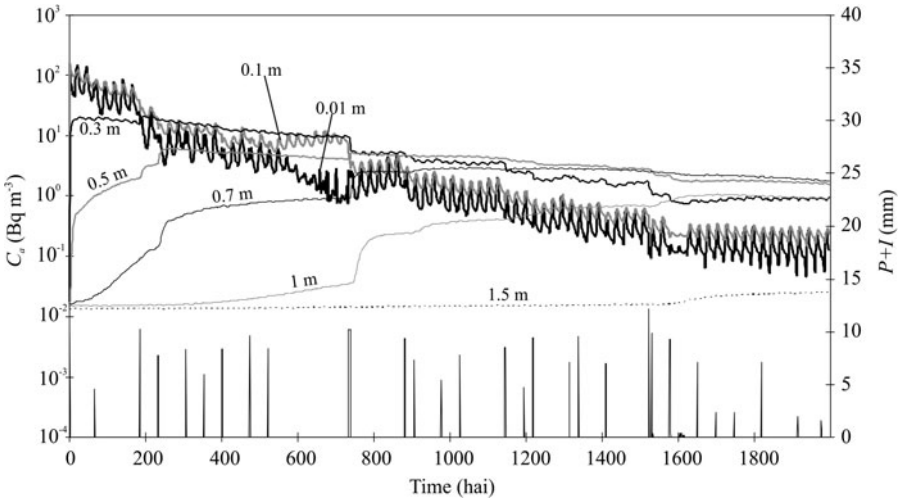

Fig. 10 Simulated HTO_g concentration in soil air at different depths for calibrated period (DAI 0-83). hai: hours after injection

5 Conclusion

Results from the presented analysis show that tritium flux from soil to atmosphere following a tracer application was one order of magnitude lower in vapor—owing to a HTO_g concentration gradient—than in liquid phase—owing to the evaporation process—for the simulated period. Field data and simulations indicate that tritium

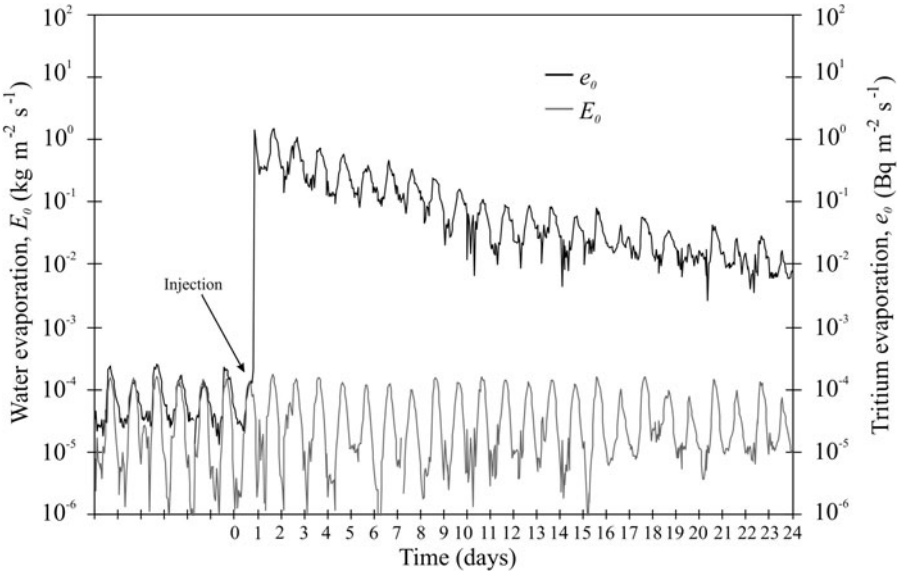

Fig. 11 Water (E_0) and tritium (e_0) evaporation from ground surface before and after tritium injection

movement primarily occurs in the liquid phase, while during drying conditions tritium movement mainly takes place as vapor phase. The difference between tritium liquid and vapor mass fluxes occurs mainly in the top soil, whereas for tritium-free water and vapor the difference is over the entire soil thickness. Advection and mechanical dispersion controlled the transport of tritium in liquid phase; molecular diffusion (effective diffusion) was the main transport process in vapor phase.

Variations of tritium gas concentration in soil are directly related to diurnal variation of meteorological parameters. The decline of concentration in the top soil during night time is reinforced by night re-emission. The sink terms of tritium as evaporation, transpiration, deep drainage and radioactive decay account for 61.51%, 34.65%, 3.13% and 0.29% tritium losses, respectively. According to modeling, tritium mass balance error was 0.5%. Evaporation and transpiration contribute meaningfully to the soil natural attenuation process at short and long term, respectively; and limited the penetration of tritiated water to a depth of no more than 2 m. After 83 days, tritium activity decreased in soil by 95%, and tritium background concentration is recovered after 429 days.

The presented model constitutes a powerful tool to evaluate tritium behavior, a common radionuclide in the surroundings areas of nuclear power stations and radioactive waste disposal facilities, in soil and vadose zone as well as to predict the soil and groundwater natural attenuation. The model can be used for transport simulation of similar isotopes considering the partitioning of isotopic species between aqueous and gaseous phase.

Acknowledgements CGL-2004-05963-C04-01 and CGL2007-66861-C04-03 research projects, Spanish Ministry of Science and Innovation. 08225/PI/08 research project, "Programa de Generación del Conocimiento Científico de Excelencia" of the Fundación Seneca, Región de Murcia (II PCTRM 2007-10).

Support for this work was provided by the Technical University of Cartagena. We also thank D. Mallants and another, anonymous, reviewer for helpful comments on the manuscript.

Appendix: Nomenclature

$()_0$	values at the ground surface
α	dimensionless water stress response function (–)
b	pore size distribution index (–)
c_E	bulk transfer coefficient for evaporation (–)
C_r	HTO_g concentration at reference height, $Bq\,m^{-3}$ air
C_a	HTO_g concentration of soil air, $Bq\,m^{-3}$ air
C_w	HTO_l concentration of soil water, $Bq\,m^{-3}$ water
D	soil water diffusivity function, $m^2\,s^{-1}$
D_T	hydrodynamic dispersion, $m^2\,s^{-1}$
D_{Ta}	molecular HTO_g diffusion coefficient in air, $m^2\,s^{-1}$
D_{Tw}	molecular HTO_l diffusion coefficient in water, $m^2\,s^{-1}$
D_{wa}	water vapor diffusion coefficient in air, $m^2\,s^{-1}$
e_e	evaporation–condensation of HTO_l in soil, $kg\,m^{-3}\,s^{-1}$
e_t	transpiration of HTO_l in soil, $kg\,m^{-3}\,s^{-1}$
E_e	evaporation–condensation of water in soil, $kg\,m^{-3}\,s^{-1}$
E_r	amount of runoff, $kg\,m^{-2}\,s^{-1}$
E_t	actual transpiration due to root water uptake, $kg\,m^{-3}\,s^{-1}$
ET_p	potential evapotranspiration, $kg\,m^{-2}\,s^{-1}$
ET_0	reference evapotranspiration, $kg\,m^{-2}\,s^{-1}$
f	ground cover sigmoid function (–)
τ_a	tortuosity for soil air (–)
τ_w	tortuosity for soil water (–)
h	pressure head, m
h_s	air entry potential, m
I	irrigation, $kg\,m^{-2}\,s^{-1}$
K	unsaturated hydraulic conductivity of soil, $m\,s^{-1}$
K_c	crop-specific coefficient (–)
K_s	saturated hydraulic conductivity of soil, $m\,s^{-1}$
λ	dispersivity, m
P	precipitation, $kg\,m^{-2}\,s^{-1}$
q	vertical liquid water flux, $kg\,m^{-2}\,s^{-1}$
q_s	maximum infiltration flux, $kg\,m^{-2}\,s^{-1}$
r_e	resistance of evaporation in soil as function of water content, s^{-1}
ρ_a	density of moist air as function of temperature, $kg\,m^{-3}$
ρ_s	bulk density of soil, $kg\,m^{-3}$
ρ_w	density of liquid water, $kg\,m^{-3}$
t	time, s
T_p	potential transpiration, $kg\,m^{-2}\,s^{-1}$
T_s	soil temperature, °K
θ	volumetric soil water content, $m^3\,m^{-3}$
θ_s	saturated volumetric soil water content, $m^3\,m^{-3}$

u_r wind speed at reference height, $\mathrm{m\,s^{-1}}$
v seepage velocity, $\mathrm{m\,s^{-1}}$
W_r specific humidity of air at reference height, $\mathrm{kg\,kg^{-1}}$
W_a specific humidity of soil air, $\mathrm{kg\,kg^{-1}}$
W_{sat} specific humidity of soil air at saturation, $\mathrm{kg\,kg^{-1}}$
z vertical space coordinate, m
z_{root} root depth, m

References

Allen RG, Pereira LS, Raes D, Smith M (1998) Crop evapotranspiration. Guidelines for computing crop water requirements. Irrigation and drainage. Paper No. 56, FAO, Rome, Italy

Al Nakshabandi G, Kohnke H (1965) Thermal conductivity and diffusivity of soils as related to moisture tension and other physical properties. Agric Meteorol 2:271–279

Andraski BJ, Stonestrom DA, Michel RL, Halford KJ, Radyk JC (2005) Plant-based plume-scale mapping of tritium contamination in desert soils. Vadose Zone J 4:819–827

Auer LH, Rosenberg ND, Birdsell KH, Whitney EM (1996) The effects of barometric pumping on contaminant transport. J Contam Hydrol 24:145–166

Barnes CJ, Jacobson G, Smith GD (1994) The distributed recharge mechanism in the Australian arid zone. Soil Sci Soc Am J 58(1):31–40

Barry PJ, Watkins BM, Belot Y, Davis PA, Edlund O, Galeriu D, Raskob W, Rusell S, Togawa O (1999) Intercomparison of the model predictions of tritium concentrations in soil and foods following acute airborne HTO exposure. J Environ Radioact 42:191–207

Bear J, Gilman A (1995) Migration of salts in the unsaturated zone caused by heating. Transp Porous Media 19:139–156

Belot Y, Watkins BM, Edlund O, Galeriu D, Guinois G, Golubev AV, Meruville C, Raskob W, Täschner M, Yamazawa H (2005) Upward movement of tritium from contaminated groundwaters: a numerical analysis. J Environ Radioact 84:259–270

BIOMOVS II (1996) Tritium in the food chain: comparison of predicted and observed behaviour. A. Re-emission from soil and vegetation. B. Formation of organically bound tritium in grain of spring wheat. Technical report No. 13, Swedish Radiation Protection Institute, 171 16 Stockholm, Sweden

Burnham KP, Anderson DR (2002) Model selection and multimodel inference: a practical information-theoretic approach, 2nd edn. Springer, New York

Campbell GS (1974) A simple method for determining unsaturated conductivity from moisture retention data. Soil Sci 117:311–314

Campbell GS, Norman JM (1998) An introduction to environmental biophysics, 2nd edn. Springer, New York

Campbell GS, Shiozawa S (1992) Prediction of hydraulic properties of soils using particle-size distribution and bulk density data. In: van Genuchten MTh et al (eds) Indirect methods for estimating the hydraulic properties of unsaturated soils. University of California, Riverside, pp 317–328

Clapp R, Hornberger G (1978) Empirical equations for some soil hydraulic properties. Water Resour Res 14(4):601–604

Cosby BJ, Hornberger GM, Clapp RB, Ginn TR (1984) A statistical exploration of the relationships of soil moisture characteristics to the physical properties of soils. Water Resour Res 20(6):682–690

Cussler EL (1997) Diffusion: mass transfer in fluid systems. Cambridge University Press, New York

Ellsworth PZ, Williams DG (2007) Hydrogen isotope fractionation during water uptake by woody xerophytes. Plant Soil 291:93–107

Feddes RA, Kowalik PJ, Zaradny H (1978) Simulation of field water use and crop yield. Wiley, New York

Garcia CA, Andraski BJ, Stonestrom DA, Cooper CA, Johnson MJ, Michel RL, Wheatcraft SW (2009) Transport of tritium contamination to the atmosphere in an arid environment. Vadose Zone J 8:450–461

Gee GW, Or D (2002) Particle size analysis. In: Dane J, Topp C (eds) Methods of soil analysis, Part 4. SSSA book series, vol 5. Am Soc Agron, Madison, pp 255–294

GNIP/IAEA (2009) International atomic energy agency. Isotopes hydrology information system. Available via ISOHIS database. http://isohis.iaea.org/. Accessed 1 April, 2008

Gran M, Carrera J, Olivella S, Saaltink MW (2011) Modeling evaporation processes in a saline soil from saturation to oven dry conditions. Hydrol Earth Syst Sci 15:2077–2089. doi:10.5194/hess-15-2077-2011

Grossman RB, Reinsch TG (2002) Bulk density and linear extensibility. In: Dane J, Topp C (eds) Methods of soil analysis, Part 4. SSSA book series, vol 5. Am Soc Agron, Madison, pp 201–228

Jackson DR, Reginato RJ, Kimball BA, Nakayama FS (1974) Diurnal soil water evaporation. Comparison of measured and calculated soil water fluxes. Soil Sci Soc Am Proc 38:861–866

Jiménez-Martínez J, Skaggs TH, van Genuchten MTh, Candela L (2009) A root zone modelling approach to estimating groundwater recharge from irrigated areas. J Hydrol 367(1–2):138–149

Joshi B, Maule C, De Jong C (1997) Subsurface hydrologic regime and estimation of diffuse soil water flux in a semi arid region. Electron J Geotech Eng. http://geotech.cive.okstate.edu/ejge/ppr9702/index.htm. Accessed 15 May, 2008

Kalisz PJ, Stringer JW, Volpe JA, Clark DT (1988) Trees as monitor of tritium in soil water. J Environ Qual 17:62–70

Kline JR, Stewart ML (1974) Tritium uptake and loss in grass vegetation which has been exposed to an atmospheric source of tritiated water. Health Phys 26:567–573

Kondo J, Saigusa N (1994) Modeling the evaporation from bare soil with a formula for vaporization in the soil pores. J Meteorol Soc Jpn 72(3):413–421

Kondo J, Xu J (1997) Seasonal variations in the heat and water balance for nonvegetated surfaces. J Appl Meteorol 36(12):1676–1695

Kroes JG, Van Damm JC (2003) Reference manual SWAP: version 3.0.3. Rep. 773. Alterra Green World Res, Wageningen, The Netherlands

Larsbo M, Jarvis N (2003) MACRO 5.0. A model of water flow and solute transport in macroporous soil. Technical description, Emergo 2003: 6, Studies in the Biogeophysical Environment, Department of Soil Sciences, Swedish University of Agricultural Sciences, Uppsala, Sweden, 47 p

Maraqa MA, Wallace RB, Voice TC (1997) Effects of degree of water saturation on dispersivity and inmobile water in sandy soil columns. J Contam Hydrol 25:199–218

Matsushima D, Kondo J (1995) An estimation of the bulk transfer coefficients for a bare soil surface using a linear model. J Appl Meteorol 34(4):927–940

Mayers CJ, Andraski BJ, Cooper CA, Wheatcraft SW, Stonestrom DA, Michel RL (2005) Modeling tritium transport through a deep unsaturated zone in arid environment. Vadose Zone J 4:967–976

McCumber MC, Pielke RA (1981) Simulations of the effects of surface fluxes of heat and moisture in a mesoscale numerical model 1 soil layer. J Geophys Res 86(C10):9929–9938

Mills R (1973) Self-diffusion in normal and heavy water in the range 1–45°. J Phys Chem 77:685–688

Milly PCD (1982) Moisture and heat transport in hysteretic, inhomogeneous porous media: a matric head-based formulation and a numerical model. Water Resour Res 18(3):489–498

Nagai H (2002) Validation and sensitivity analysis of a new atmosphere-soil-vegetation model. J Appl Meteorol 41:160–176

Overman AR, Scholtz RV (2002) Mathematical models of crop growth and yield. Dekker, New York

Pachepsky YA, Smettem KRJ, Vanderborght J, Herbst M, Vereecken H, Wosten JHM (2004) Reality and fiction of models and data in soil hydrology. In: Feddes RA et al (ed) Unsaturated-zone modeling. Kluwer Academic, Dordrecht

Parker JC (2003) Physical processes affecting natural depletion of volatile chemicals in soil and groundwater. Vadose Zone J 2:222–230

Philip JR, de Vries DA (1957) Moisture movement in porous materials under temperature gradients. EOS Trans AGU 38(2):222–232

Phillips FM (1994) Environmental tracers for water movement in desert soils of the American Southwest. Soil Sci Soc Am J 58:15–24

Pruess KA Oldenburg C Moridis G (1999) TOUGH2 user's guide version 2.0. EO Lawrence Berkeley National Laboratory report LBNL-43134, Lawrence Berkeley Natl Lab, Berkeley, California

Raskob W (1995) Assessment of the environmental-impact from tritium releases under normal operation conditions and after accidents. Fusion Technol 28:934–939

Richard WH, Kirby LJ (1987) Trees as indicators of subterranean water flow from a retired radioactive waste disposal site. Health Phys 52:201–206

Richard WH, Price KR (1989) Uptake of tritiated groundwater by black locust trees. Northwest Sci 63:87–89

Roy WR, Krapac IG, Chou SFJ, Griffin RA (1991) Batch-type procedures for estimating soil adsorption of chemicals. Rep No US EPA/530-SW-87-006-F, US Environmental Protection Agency, Cincinnati

Scanlon BR (1992) Evaluation of liquid and vapor water flow in desert soils based on chlorine 36 and tritium tracers and nonisothermal flow simulations. Water Resour Res 28(1):285–297

SIAM (2008) Servicio de Información Agraria de Murcia. Climatology data. Available via http://siam.imida.es. Accessed 15 September 2009

Šimunek J, van Genuchten MTh, Šejna M (2005) The HYDRUS-1D software package for simulating the movement of water, heat, and multiple solutes in variability saturated media, version 3.0. Department of Environmental Sciences University of California Riverside, Riverside, California, USA, 270 p

Täschner M, Bunnenberg C, Camus H, Belot Y (1995) Investigations and modelling of tritium re-emissions from soil. Fusion Technol 28:976–981

Täschner M, Bunnenberg C, Raskob W (1997) Measurements and modeling of tritium reemission rates after HTO depositions at sunrise and at sunset. J Environ Radioact 36:219–235

Thatcher LL, Janzer VJ, Edwards KW (1977) Methods for determination of radioactive substances in water and fluvial sediments. USGS techniques of water resources investigations. Book 5, Chap A5. US Gov Print Office, Washington, DC

Taylor SA, Ashcroft GM (1972) Physical edaphology. Freeman, San Francisco, pp 434–435

Wesseling JG, Elbers JA, Kabat P, van den Broek BJ (1991) SWATRE: instructions for input. Internal note, Winand Staring Centre, Wageningen, The Netherlands

Yamazawa H (2001) A one-dimensional dynamical soil atmosphere tritiated water transport model. Environ Model Softw 16:739–751

Yamazawa H, Nagai H (1997) Development of one-dimensional atmosphere-bare soil model. JAERI-Data/Code 97-401